

## Identification of $I_{K_r}$ Kinetics and Drug Binding in Native Myocytes

QINLIAN ZHOU,<sup>1</sup> ANDREW C. ZYGMUNT,<sup>2</sup> JONATHAN M. CORDEIRO,<sup>2</sup> FERNANDO SISO-NADAL,<sup>1</sup>  
ROBERT E. MILLER,<sup>1</sup> GREGERY T. BUZZARD,<sup>3</sup> and JEFFREY J. FOX<sup>4</sup>

<sup>1</sup>Gene Network Sciences, 58 Charles Street, Cambridge, MA 02141, USA; <sup>2</sup>Masonic Medical Research Laboratory, 2150 Bleecker Street, Utica, NY 13501, USA; <sup>3</sup>Department of Mathematics, Purdue University, West Lafayette, IN 47907, USA; and <sup>4</sup>Center for Applied Mathematics, Cornell University, Ithaca, NY 14853, USA

(Received 16 October 2008; accepted 27 March 2009; published online 8 April 2009)

**Abstract**—Determining the effect of a compound on  $I_{K_r}$  is a standard screen for drug safety. Often the effect is described using a single  $IC_{50}$  value, which is unable to capture complex effects of a drug. Using verapamil as an example, we present a method for using recordings from native myocytes at several drug doses along with qualitative features of  $I_{K_r}$  from published studies of HERG current to estimate parameters in a mathematical model of the drug effect on  $I_{K_r}$ .  $I_{K_r}$  was recorded from canine left ventricular myocytes using ruptured patch techniques. A voltage command protocol was used to record tail currents at voltages from  $-70$  to  $-20$  mV, following activating pulses over a wide range of voltages and pulse durations. Model equations were taken from a published  $I_{K_r}$  Markov model and the drug was modeled as binding to the open state. Parameters were estimated using a combined global and local optimization algorithm based on collected data with two additional constraints on  $I_{K_r}$   $I$ - $V$  relation and  $I_{K_r}$  inactivation. The method produced models that quantitatively reproduce both the control  $I_{K_r}$  kinetics and dose dependent changes in the current. In addition, the model exhibited use and rate dependence. The results suggest that: (1) the technique proposed here has the practical potential to develop data-driven models that quantitatively reproduce channel behavior in native myocytes; (2) the method can capture important drug effects that cannot be reproduced by the  $IC_{50}$  method. Although the method was developed for  $I_{K_r}$ , the same strategy can be applied to other ion channels, once appropriate channel-specific voltage protocols and qualitative features are identified.

**Keywords**—Mathematical modeling, Drug-ion current interaction, Parameter estimation, Global optimization, Verapamil, Cardiac electrophysiology.

### INTRODUCTION

Pharmacological interference of ion channels, whether designed or unintended, can modify channel behavior and alter cellular and tissue electrical prop-

erties.<sup>38</sup> Modification of cardiac activity is of particular concern for drug safety testing, due to potential proarrhythmic effects of candidate compounds.<sup>16</sup> For example, the rapid delayed rectifier potassium current  $I_{K_r}$  is inhibited by a large number of pharmacological agents,<sup>10</sup> some of which have been found to be proarrhythmic in certain patients and have therefore been withdrawn from the market.<sup>12</sup> Scientists have identified KCNH2 (commonly referred to as HERG—Human Ether a go go Related Gene) as the gene that expresses the channel-forming protein through which the  $I_{K_r}$  current passes.<sup>40,48</sup> Hence, determining the effect of a compound on the HERG current in cell expression systems is a common early drug safety screen.<sup>15</sup> Typically the HERG current is recorded under control and then under several concentrations of the candidate compound, often using a simple single step voltage clamp protocol.<sup>3,5,37</sup> The effect of the drug on the HERG current is usually reported by an  $IC_{50}$  value,<sup>36</sup> which is the concentration of the drug at which the peak tail current is reduced by 50%. Although these HERG screens can be completed quickly, and high-throughput screening technologies are available,<sup>25</sup> there are at least three shortcomings in using a single  $IC_{50}$  value from a HERG screen to describe the effect of a compound on  $I_{K_r}$ . First, quantitative differences between the HERG current and  $I_{K_r}$  recorded in native myocytes have been reported.<sup>11</sup> It remains unclear how to translate an  $IC_{50}$  value measured in a HERG expression system to a corresponding  $IC_{50}$  value for  $I_{K_r}$  in myocytes. Second, recent experimental<sup>24</sup> and computational<sup>35</sup> studies have shown that the measured  $IC_{50}$  value can depend on the particular voltage clamp protocol used to measure the current. Thus, comparing results from tests using different protocols is difficult. Third, it is known that drug block may not only reduce the peak tail current, but also change the channel kinetics.<sup>43</sup> Given the complex and rate-dependent interplay between ion currents during the cardiac

Address correspondence to Qinlian Zhou, Gene Network Sciences, 58 Charles Street, Cambridge, MA 02141, USA. Electronic mail: qzhou@gnsbiotech.com

action potential, these kinetic effects may be important in determining the potential pro-arrhythmic effects of a compound.<sup>39</sup>

Mathematical models have a long and rich history in electrophysiology.<sup>17,18,31</sup> These models serve as compact representations for quantifying ion current properties and are useful tools for helping to elucidate the roles of currents in determining cellular electrical activity.<sup>14,19,21,41,47</sup> A common approach for modeling the concentration-dependent effect of a compound on an ion current is to modify the channel conductance by the Hill equation, in which an  $IC_{50}$  value measured from experiments is used to calculate the fractional reduction in current magnitude as a function of drug concentration.<sup>5</sup> Due to limitations of the  $IC_{50}$  method mentioned above, this method is not able to capture quantitative changes in channel kinetics induced by a compound.

Another approach for modeling the effects of drug–channel interaction on an ion current is to use a Markov representation of the ion channel, and model the drug as binding to specific channel states.<sup>6,44</sup> Such a model captures the physical interaction of the compound with the channel protein and is able to reproduce a range of dynamic behaviors that are beyond the reach of the  $IC_{50}$  method. However, since the binding properties of a compound as well as the transition rates between different channel states are usually unknown and difficult to obtain, using a Markov representation of drug-binding requires the estimation of a large number of parameters, which presents a significant model identification problem. A common strategy for estimating parameters in complex models is to define a “cost function”, which is a measure of the discrepancy between the “training data”, a time series of collected experimental data, and the model output. Parameters are then estimated by using an optimization algorithm to find parameter values that minimize the cost function.<sup>32,42</sup>

Many computationally efficient local optimization methods are available, but these rely heavily on good initial guesses for parameters if the cost landscape has many local minima.<sup>32</sup> Alternatively, global methods can be used to search throughout a wider range of parameter space,<sup>13</sup> although there is no guarantee of finding a global minimum. These global methods often produce many parameter sets that can reproduce the training data, but that produce very different behaviors under other conditions, such as other voltage clamp protocols. A straightforward way to constrain  $I_{Kr}$  model parameters in such a circumstance is to collect data under additional voltage clamp protocols. For example, Milescu *et al.* suggest that analyzing data generated by complex stimulation protocols could improve a maximum likelihood estimation method for

model identifiability.<sup>30</sup> However, it is often difficult to collect enough data to constrain the problem in native myocytes, due to contamination from other cardiac ion channels and to current rundown if very long protocols are used. We study an alternative approach that uses qualitative features from HERG experiments to help constrain parameter estimation.

We present here a systematic method for developing detailed models of the effects of a compound on  $I_{Kr}$ . We use a Markov representation of the ion channel, and model the drug as binding to specific channel states. The method involves the following steps:

1. Record  $I_{Kr}$  in native myocytes under control and several concentrations of the drug under study using a complex voltage protocol that covers a wide range of voltages and pulse durations.
2. Gather qualitative features from published studies of the HERG channel in transfected cell lines and enforce those features that the  $I_{Kr}$  model is expected to reproduce.
3. Use a combined global and local optimization strategy to estimate model parameters by minimizing a cost function that includes not only the time series data from step 1, but also the qualitative features from step 2.

Using this approach, one can find optimal parameters that allow drug– $I_{Kr}$  models to quantitatively reproduce both the control  $I_{Kr}$  kinetics and concentration-dependent drug effects. Moreover, the models thus generated conform to commonly accepted features of  $I_{Kr}$ /HERG current. The method was tested using  $I_{Kr}$  data recorded from canine ventricular myocytes in the presence of verapamil, a known  $I_{Kr}$  inhibitor.<sup>34,52</sup> Verapamil is a particularly interesting test case; although it inhibits  $I_{Kr}$ , it does not appear to have pro-arrhythmic effects in patients.<sup>36</sup> The results suggest that: (1) the technique proposed here has the practical potential to develop data-driven models that quantitatively reproduce channel behavior in native myocytes; (2) the method can capture important drug effects, such as rate- and use-dependence, that cannot be reproduced by the  $IC_{50}$  method. Although the method was developed for  $I_{Kr}$ , the same strategy can be applied to other ion channels, once appropriate channel-specific voltage protocols and qualitative features are identified.

## METHODS

### *Voltage Clamp Data*

#### *Isolated Myocyte Preparation*

Myocytes from epicardial, midmyocardial, and endocardial regions were prepared from canine hearts

using techniques described previously.<sup>8,9</sup> Briefly, male and female adult mongrel dogs were anesthetized with sodium pentobarbital (35 mg/kg i.v.), their hearts were rapidly removed and placed in nominally  $\text{Ca}^{2+}$ -free Tyrode's solution. A wedge consisting of the left ventricular free wall supplied by a descending branch of the circumflex artery was excised, cannulated and perfused with nominally  $\text{Ca}^{2+}$ -free Tyrode's solution containing 0.1% BSA for a period of 5 min. The wedge preparations were then subjected to enzyme digestion with the nominally  $\text{Ca}^{2+}$ -free solution supplemented with 0.5 mg/mL collagenase (Type II, Worthington), 0.1 mg/mL protease, and 1 mg/mL BSA for 8–12 min. After perfusion, thin slices of tissue from the epicardium (<2 mm from the epicardial surface), midmyocardial (~5–7 mm from the epicardial surface), and endocardium (<2 mm from the endocardial surface) were shaved from the wedge using a dermatome. The tissue slices were then placed in separate beakers minced and incubated in fresh buffer containing 0.5 mg/mL collagenase, 1 mg/mL BSA and agitated. The supernatant was filtered, centrifuged, and the pellet containing the myocytes was stored at room temperature. All animal procedures were in accordance with previously established guidelines (NIH publication No. 85-23, revised 1985).

### Solutions

The nominally  $\text{Ca}^{2+}$ -free solution has the following composition (mM): NaCl 135, KCl 5.4,  $\text{MgCl}_2$  1.0,  $\text{NaH}_2\text{PO}_4$  0.33, glucose 10, HEPES 10, pH = 7.4 with NaOH. The enzyme solution has the same composition except that it also contains 0.5 mg/mL collagenase (Type II, Worthington) and 0.1 mg/mL protease (Type XIV, Sigma). For electrophysiological recordings, ventricular cells were superfused with a HEPES buffer of the following composition (mM): NaCl 140, KCl 4.0,  $\text{MgCl}_2$  1.0,  $\text{CaCl}_2$  2.0, HEPES 10, and glucose 10. pH adjusted to 7.4 with NaOH. The patch pipette solution had the following composition (mM): K-aspartate 125, KCl 10,  $\text{MgCl}_2$  1.0, EGTA 5, MgATP 5, HEPES 5, NaCl 10. pH = 7.2 with KOH.

### Electrophysiology

All experiments were performed at 37 °C. Cells were placed in a temperature controlled chamber (PDMI-2, Medical Systems Corp.) mounted on the stage of an inverted microscope (Nikon TE300). Voltage clamp and conventional recordings were made using a MultiClamp 700A amplifier and MultiClamp Commander (Axon Instruments). Patch pipettes were fabricated from borosilicate glass capillaries (1.5 mm O.D., Fisher Scientific, Pittsburg, PA). The pipettes were pulled using a gravity puller (Model PP-830, Narashige Corp.) and the pipette resistance ranged from 1 to 4 M $\Omega$  when filled with the internal solution. After a whole cell patch was established, cell capacitance was measured by applying -5 mV voltage steps.  $I_{\text{Kr}}$  was measured as the time-dependent tail current measured at various potentials following depolarizing pulses of variable time and duration (Fig. 1). For  $I_{\text{Kr}}$  recordings, HMR1556 (100 nM) an inhibitor of the slow delayed rectifier potassium current  $I_{\text{Ks}}$ , was added to the recording solutions. In addition, 300  $\mu\text{M}$   $\text{CdCl}_2$  was added to the recording solutions to inhibit L-type  $\text{Ca}^{2+}$  current. A four-barrel quartz micromanifold (ALA Scientific Instruments Inc., Westbury, NY) placed 200  $\mu\text{m}$  from the cell was used to apply verapamil at various concentrations.

Electronic compensation of series resistance to 60–70% was applied to minimize voltage errors. All analog signals (cell current and voltage) were acquired at 10 kHz, filtered at 2–5 kHz, digitized with a Digi-data 1322A converter (Axon Instruments) and stored using pClamp9 software.

Figure 1 shows the voltage protocol used in this study. It is designed to expose the drug-channel interaction by measuring voltage-dependent changes in  $I_{\text{Kr}}$  tail currents, and time- and voltage-dependent changes in  $I_{\text{Kr}}$  activation.

### Markov Model Formulation

The Markov model we studied is a set of coupled ordinary differential equations that follows the five

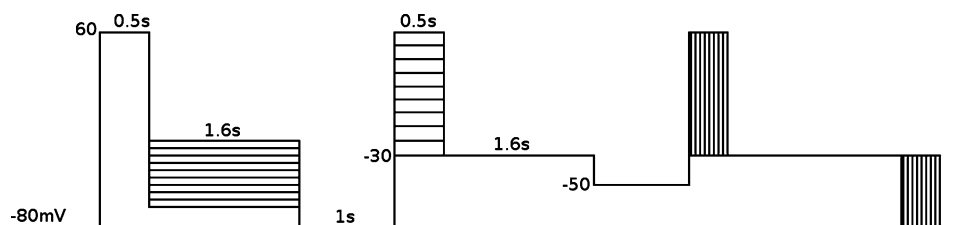


**FIGURE 1.** The voltage protocol used in this study consists of 10 sweeps, each with three components. The first component measures tail currents at voltages from -20 to -65 mV in 5 mV decrements. The second segment tests tail current after depolarization to voltages from 60 to -30 mV in 10 mV decrements. The third is an envelope of tails protocol with depolarization duration from 10 to 370 ms in 40 ms increments.

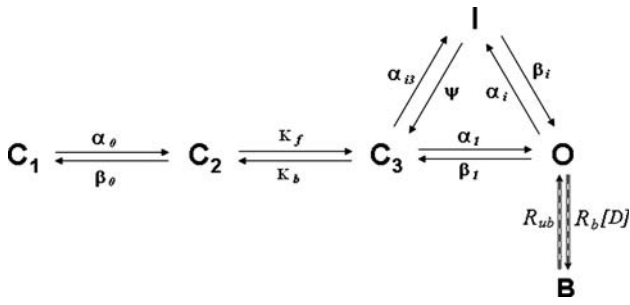


**FIGURE 2.** State diagram of the  $I_{Kr}$  Markov model structure. Arrows refer to transitions between states. The rate constants are shown above (below) the arrows.

state formulation given in Mazhari *et al.*<sup>29</sup> with three closed states ( $C_1$ ,  $C_2$ , and  $C_3$ ), one open state ( $O$ ), and one inactive state ( $I$ ) (Fig. 2). In this formulation, each state variable represents the fraction of channels in a particular conformation. The channel only conducts current in the open state. At rest, the channels are in a closed state. Following a depolarizing change in membrane potential, the channels will be activated (changing from closed to open) and will conduct current. After sustained activation the channel will be inactivated (changing from open to inactive) and become non-conducting.

The Mazhari model is a detailed and widely used model of  $I_{Kr}$ , and therefore an appropriate model for study. The model was based on experimental studies of ferret  $I_{Kr}$ <sup>26</sup> and HERG current in transfected cells.<sup>50</sup> Liu *et al.*<sup>26</sup> showed that activation of  $I_{Kr}$  involved one voltage sensitive step and one voltage insensitive step, and therefore proposed a model with voltage-independent rate constants between two closed states. Wang *et al.* found that at least three closed states were required to reproduce the sigmoidal onset of the activation of the heterologously expressed HERG current.<sup>50</sup> The Mazhari *et al.* model also incorporated single channel studies on HERG current that provided evidence for closed-state inactivation.<sup>23</sup> The model has been used in other studies,<sup>27</sup> including published investigations of a detailed model of the human ventricular action potential<sup>21</sup> and a model of the canine ventricular myocyte.<sup>46</sup> All state transition rates except for  $K_f$  and  $K_b$  (rates between  $C_2$  and  $C_3$ ) are exponential functions of voltage:  $p_x e^{p_y V}$ , where  $p_x$  and  $p_y$  are parameters in  $\text{ms}^{-1}$  and  $\text{mV}^{-1}$ , respectively, and  $V$  is the membrane potential in mV. To satisfy the microscopic reversibility condition,  $\psi$  is defined as:  $\psi = (\beta_1 \beta_i \alpha_{i3}) / (\alpha_1 \alpha_i)$ . Results presented here consider drug binding to the open state.<sup>52</sup> The drug-bound state is given by  $B$ . The binding rate is  $R_b[D]$  where  $[D]$  is the drug concentration in  $M$  (mol/L) and  $R_b$  is in  $\text{ms}^{-1} M^{-1}$ , and the unbinding rate is  $R_{ub}$  in  $\text{ms}^{-1}$ . All parameters for the transition rates are estimated using

the optimization strategy described in section “Parameter Estimation Strategy”.

The macroscopic  $I_{Kr}$  current is calculated using the Goldman–Hodgkin–Katz (GHK) current equation<sup>22</sup>:

$$I_{Kr} = OP_K \frac{F^2}{RT} V \frac{(A_c [K_i] - [K_o] e^{-VF/RT})}{1 - e^{-VF/RT}} \quad (1)$$

Here  $P_K$  is the permeability of the membrane to potassium ions, and  $[K_i]$  ( $[K_o]$ ) is the concentration of potassium ions inside (outside) of the cell.  $F$  is the Faraday’s constant (96.5 K coulomb/mol),  $R$  the ideal gas constant (8314 J/mol), and  $T$  is the temperature (310 K). The parameter  $A_c$  is the activity coefficient, which accounts for the fact that the thermodynamic activity of an electrolyte in solution is lower than the chemical concentration because each ion is slightly less available at finite concentration than at infinite dilution.<sup>17</sup>  $[K_i]$  and  $[K_o]$  are estimated to be 120 and 4 mM, respectively.

### Parameter Estimation Strategy

To estimate parameters in the model, we use a combined global and local optimization algorithm described in section “Optimization Algorithm” to minimize a cost function  $F(\mathbf{M})$  made up of three terms.

$$F(\mathbf{M}) = w_1 f_1(\mathbf{M}) + w_2 f_2(\mathbf{M}) + w_3 f_3(\mathbf{M}) \quad (2)$$

Here  $\mathbf{M}$  is a vector made up of the parameters in the model to be estimated. The following three sections describe each of the three terms in Eq. (2). The first term compares the model results to the acquired patch clamp data, the second term compares the qualitative shape of the model’s current–voltage ( $I$ – $V$ ) relationship to that measured in HERG channels, and the third term compares the model’s inactivation properties to qualitative features of HERG channels.  $w_1$ ,  $w_2$ , and  $w_3$  are the weights for each term.  $f_1(\mathbf{M})$ , which measures the difference between model and data, is a general term that is likely to be included in estimating parameters for any ion current model. The other two terms,  $f_2(\mathbf{M})$  and  $f_3(\mathbf{M})$ , are designed specifically for  $I_{Kr}$ , as described in the sections below. Studies of other ion currents would likely need different terms that incorporate appropriately chosen qualitative features.  $f_2(\mathbf{M})$  and  $f_3(\mathbf{M})$  are calculated for control conditions only. Thus, the drug concentration is set to 0 when calculating these terms.  $f_1(\mathbf{M})$  includes the difference between model and data both in control and in the presence of the drug. The weights are chosen to balance the trade-off between matching particular experimental  $I_{Kr}$  recordings and reproducing important qualitative features of the current. For convenience, we choose  $w_1 = 1$ . The other weights are defined below.



The goal of the optimization process is to find parameter sets that minimize the cost by iteratively changing the parameter values and evaluating all three terms until the simulation for a given parameter set nearly matches the experimental data and reproduces the two qualitative features.

### Term 1: Training Data

The first term in the cost function is defined by

$$f_1(\mathbf{M}) = \frac{\sum_{i=1}^N (\text{Train}_{\text{data}_i} - \text{Sim}_{\text{data}_i}(\mathbf{M}))^2}{2N} \quad (3)$$

Here  $\text{Train}_{\text{data}_i}$  is the training data at the  $i$ th time point,  $\text{Sim}_{\text{data}_i}(\mathbf{M})$  is the simulation value at the  $i$ th time point using the parameters given by  $\mathbf{M}$ . The sum is taken over  $i = 1$  to  $N$ , the total number of time points in the recording. The factor of 2 is only for notational convenience.

For each cell sample, we run three iterations of the protocol described in section “Electrophysiology”. The first iteration is recorded in the control condition, and the drug is applied at the beginning of the second iteration. The training data consist of current recorded during the first and the third iterations, representing current under control condition and current under steady state drug effect, respectively.

Four processing steps are used to convert the raw time series data recorded under the complex protocol described in section “Electrophysiology” to the training data in Eq. (3). First, data collected during all depolarization pulses and at  $-80$  mV are removed, since the recorded current at these voltages is contaminated by other ion currents. Hence for each sweep, only the three tail currents are used for the training data. Second, the dramatic change in voltage at step transitions induces a capacitive transient that renders the first few milliseconds of data unusable. Therefore,

the first 7–20 ms (depending on the size of the transient) of data after all step transitions are discarded from the tail currents. Third, to account for any offset in the recording, the tail currents are shifted so that the average of the last 100 data points at the end of each tail current is zero. Finally, data are resampled to reduce the number of data points, which significantly reduces the time needed to evaluate the cost function. For each tail current, the sampling rate of the training data varies according to the following sequence: 5 KHz sampling for the interval between 0 and 30 ms from the beginning of the tail current; 1 KHz sampling between 30 and 100 ms; 500 Hz sampling between 100 and 800 ms; and 125 Hz for the rest of the tail current.

To generate model output, three iterations of the voltage clamp protocol used in the experiments are applied to the model. A step function is used for the drug concentration time series. During the first iteration of the voltage clamp protocol the drug concentration is zero. During the second and third iterations the concentration of the drug is held at a fixed level to match that used in the experiment.

### Term 2: $I$ - $V$ -curve

The second term in the cost function is defined by:

$$f_2(\mathbf{M}) = \frac{1}{N_i + N_j} \left( \sum_{i=1}^{N_i} (O_i - 0.8)^2 H(0.8 - O_i) + \sum_{j=1}^{N_j} (O_j - 0.1)^2 H(O_j - 0.1) \right) \quad (4)$$

where  $H(x)$  is the Heaviside step function.  $O_i$  and  $O_j$  are the occupation probability of the open state at different voltage levels.  $N_i$  and  $N_j$  are the number of selected voltage levels where the open probability is measured. This term is evaluated by simulating the model under a standard  $I$ - $V$  protocol.<sup>29</sup> For example, Fig. 3a shows the  $I$ - $V$  curve obtained by simulating

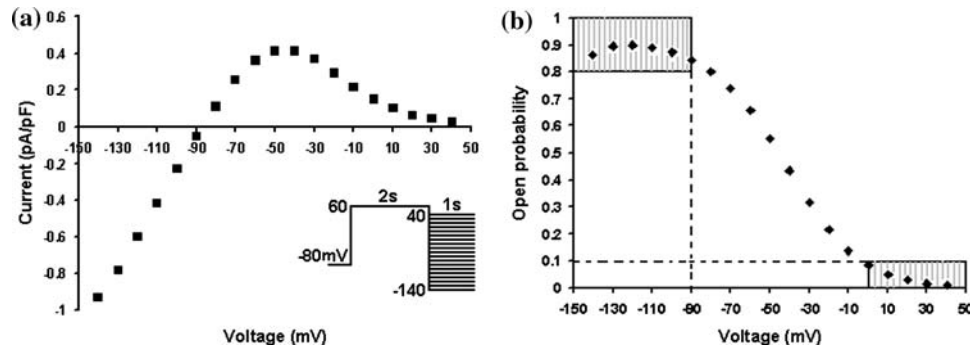


**FIGURE 3.**  $I$ - $V$  and open probability-voltage curves from the published Mazhari model.<sup>29</sup> (a) Peak tail currents were obtained under the protocol shown in inset and plotted as a function of voltage. (b) Peak open state values under the same protocol plotted vs. voltage. The shaded areas represent qualitative constraints used during optimization.

the Mazhari  $I_{Kr}$  model, which was developed to reproduce data from HERG expression systems, under the protocol shown in the inset. While the quantitative details of the  $I-V$  curve as measured in expression systems are likely different from the behavior of native canine  $I_{Kr}$ , it is widely thought that the native  $I_{Kr}$  has a similarly shaped  $I-V$  curve to that of the HERG current. Specifically, for voltages below  $-90$  mV, the current should be negative and approximately proportional to the driving force; for voltages above  $0$  mV, the current should be close to zero. Since the current is determined by the product of the open probability and the driving force, we require the open probability to be close to 1 at voltages below  $-90$  mV and close to 0 at voltages over  $0$  mV (Fig. 3b). Therefore we set  $N_i = 6$ , corresponding to voltages from  $-140$  to  $-90$  mV (in  $10$  mV intervals) in the  $I-V$  protocol, and measure  $O_i$  for each voltage level. If  $O_i \geq 0.8$ , the requirement is satisfied and no cost is added. If  $O_i < 0.8$ , then the parameter set  $\mathbf{M}$  will be penalized by adding a cost given by the square of the difference between  $O_i$  and  $0.8$ . Similarly, we set  $N_j = 5$  corresponding to voltages from  $0$  to  $40$  mV (in  $10$  mV intervals) and measure  $O_j$  for each voltage. If  $O_j \leq 0.1$ , the requirement is satisfied and no cost is added. If  $O_j > 0.1$ , the parameter set  $\mathbf{M}$  will be penalized by adding a cost given by the square of the difference between  $O_j$  and  $0.1$ .  $f_2(\mathbf{M})$  is normalized by the total number of voltage levels tested. The specific levels used are chosen for convenience. Because the  $I-V$  relation is a very important feature of the current, we choose a large weight given by  $w_2 = N_i + N_j$ .

### Term 3: Inactivation

The third term in the cost function is defined by:

$$f_3(\mathbf{M}) = \frac{1}{2(N_i - 1)} \left( \sum_{i=2}^{N_i} H(P_{i-1} - P_i) + \sum_{i=2}^{N_i} H(T_i - T_{i-1}) \right) \quad (5)$$

where  $H(x)$  is the Heaviside step function.  $P_i$  is the peak tail current after depolarizing voltage steps to different values.  $T_i$  is the value of the tail current  $50$  ms after depolarizing voltage steps to the same values.  $N_i$  is the number of selected voltage levels in the range between  $-40$  and  $60$  mV where  $P_i$  and  $T_i$  are tested. In this study,  $N_i$  is set to  $5$ , corresponding to the following voltage levels:  $-40$ ,  $0$ ,  $20$ ,  $40$ , and  $60$  mV. Experiments with HERG channels have shown that under a standard inactivation protocol (see Fig. 4a), the tail current decays more rapidly with increasing voltage.<sup>2</sup> We found that some parameter sets that were obtained by minimizing a cost function that included only the first two terms in Eq. (2) did not reproduce this qualitative feature. An example is shown in Fig. 4b, where the tails at higher voltage have higher peaks but do not decay faster and therefore have higher steady state values. In order to eliminate models with unphysiological inactivation properties, we simulate the model for a given parameter set under the inactivation protocol and measure the peak tail currents and the values of the tail current  $50$  ms after the depolarizing voltage steps mentioned above. If a peak  $P_i$  is bigger than the previous peak ( $P_{i-1}$ ), no cost is incurred. Otherwise a cost of  $1$  is added. If  $T_i$  is smaller than the previous tail

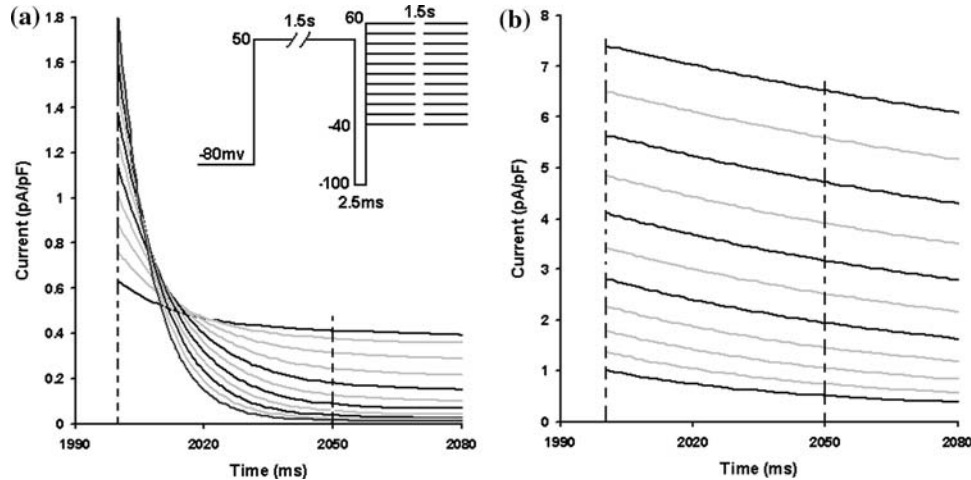


FIGURE 4. Channel inactivation. Inset shows the protocol used to test inactivation at different voltages. (a) Tail currents generated by the published Mazhari model.<sup>29</sup> At higher test voltages, the tail current has a higher peak but decays faster. (b) Tail currents generated by a model that resulted from fitting to data using only the first two terms in Eq. (2). Tail currents at higher voltages do not decay faster. In both (a) and (b), the black traces represent the currents used in calculating the third term of the cost function. The two dashed lines show where peaks ( $P_i$ ) and tails ( $T_i$ ) are obtained.

value ( $T_{i-1}$ ), no cost is incurred. Otherwise a cost of 1 is added. The total cost  $f_3(\mathbf{M})$  is normalized by the total number of comparisons. Its weight  $w_3$  is defined as  $0.01 \times 2(N_i - 1)$ . The factor 0.01 is included because the noise level of the raw data is on the order of 0.001 or less. In general, this weight should be chosen to be larger than the noise of the data so that a parameter set  $\mathbf{M}$  that does not have correct inactivation properties would be eliminated from consideration.

In experimental studies of  $I_{Kr}$  or HERG, the following standard features are usually characterized: activation,  $I-V$  relation, inactivation, recovery from inactivation, and deactivation. After using the  $I-V$  relation and inactivation as additional constraints in the optimization, the resulting models produce proper activation, deactivation, and recovery from inactivation properties. Hence, the two terms ( $f_2(\mathbf{M})$  and  $f_3(\mathbf{M})$ ) used here can be considered comprehensive qualitative constraints for  $I_{Kr}$ .

### Optimization Algorithm

The optimization routine uses a combination of global and local methods. The global method, Differential Evolution,<sup>45</sup> uses the following strategy. A population of parameter sets is generated randomly, and the cost of each parameter set is evaluated. New parameter sets are generated by first adding a weighted difference between two randomly selected parameter sets to a third random parameter set, and then by exchanging a fraction of the resulting parameter set with a member of the population according to a crossover probability. The cost of the new parameter set is then evaluated and compared to the cost of a randomly chosen set in the population. The lower cost set is kept in the next generation of the population. The optimization strategy consists of using Differential Evolution for a total of four thousand generations. After each thousand generation, the Levenberg–Marquardt<sup>28,33</sup> local method is applied to each parameter set in the population to quickly take each parameter set to a local minimum. Optimizations using more generations (for example, 5000 generations) were tested and the lowest cost did not improve significantly after 4000 generations (results not shown). Changing the random seed used by the Differential Evolution algorithm does not qualitatively change the results of the optimization (see Data Supplement).

Optimization using Differential Evolution yields many parameter sets, each with an associated cost. The lowest cost parameter set is typically considered the “best fit” to the data. However, often several parameter sets appear to reproduce the training data. Therefore, we define a cutoff value of the cost function by determining the expected fluctuations in cost due to

experimental noise (details in Appendix). Parameter sets with a cost less than this cutoff value are accepted for further analysis.

### Simulation Details

All simulations and optimizations were run on a Dell Inspiron 9100 computer and a 16-node Linux cluster of Intel Xeon dual processors using custom written C++ computer code. Each model is represented by a set of differential equations of the form  $dx/dt = f(x, t, \mathbf{M})$ , where  $\mathbf{x}$  is a vector describing the current state of the system,  $t$  is time, and  $\mathbf{M}$  is a vector of model parameters. Because the model we studied is linear for a constant value of  $V$  and  $[D]$ , we can find solutions on the time intervals between changes in  $V$  or  $[D]$  by computing the eigenvalues and eigenvectors of the system.<sup>49</sup> We use automatic differentiation to calculate the Jacobian derivative of the function  $f$ . Optimization requires about 12 h on the Linux cluster.

## RESULTS

### Testing Parameter Identifiability

To illustrate the impact of the complex protocol and the qualitative features on parameter estimation, we estimate parameters in the control  $I_{Kr}$  model using three different cost functions. The first cost function uses training data chosen to be similar to data from standard protocols. We extract two control tail currents measured at  $-30$  mV after voltage steps from  $-80$  mV to 60 and 20 mV, respectively, which are similar to protocols used in previous studies.<sup>3</sup> No qualitative features are included. The second cost function uses training data from the full complex protocol; again, no qualitative features are included. The third cost function uses training data from the complex protocol as well as the two qualitative features as described in the method section. Figure 5 shows results from the three cases. For the first case, 71 parameter sets are accepted. However, we only show 5 best parameter sets for clarity. In the third case, five parameter sets are accepted, and for the second example three are accepted. Panel a shows the activation curve (top), the  $I-V$  curve (middle) and currents under a simple step pulse (bottom) for the accepted parameter sets using the first cost function. Voltage protocols are shown as insets in each panel. Although all five parameter sets resulting from optimization reproduce the training data, none of the parameter sets produce physiological  $I_{Kr}$  currents: the activation curves appear abnormal at voltages higher than 20 mV, the  $I-V$  curves exhibit little rectification at

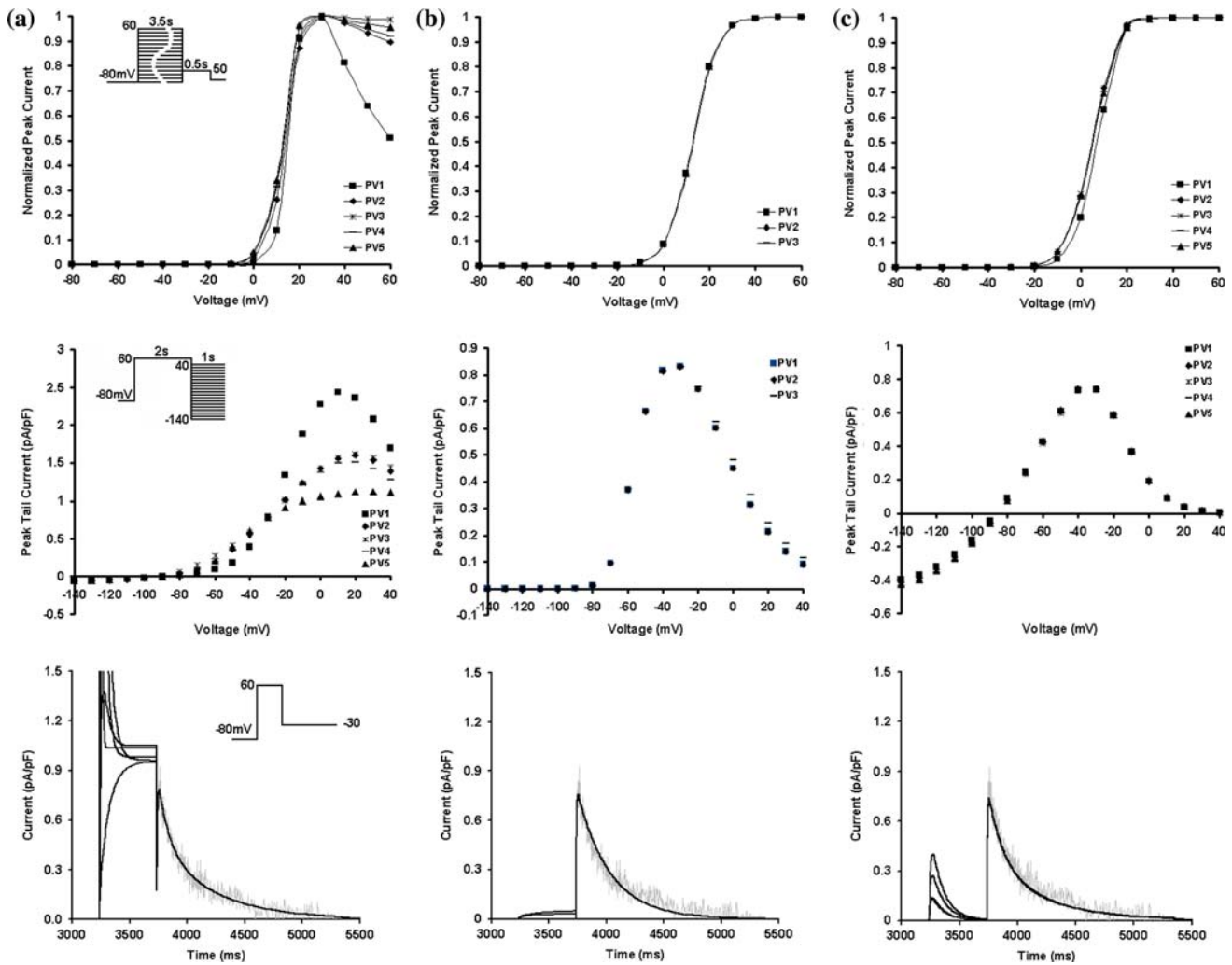


**FIGURE 5.** Comparison of models resulting from three different cost functions. Top panels: voltage dependent activation (normalized peak tail currents under protocol in inset). Middle panels:  $I$ - $V$  relations (peak tail currents under protocol in inset). Bottom panels: model-generated  $I_{K_r}$  (dark lines) and data (light curves) under a simple pulse (shown in inset). (a) 5 accepted models from fitting to data under a simplified two pulse protocol show non-physiological behavior and significant divergence. (b) 3 accepted models from fitting to data under the complex protocol are almost identical but show non-physiological  $I$ - $V$  relations. (c) 5 accepted models from fitting to data under the complex protocol plus the two qualitative constraints.

higher voltages, and currents under the step pulse to 60 mV are unphysiological. Panel b shows features of the three acceptable parameter sets resulting from the second cost function. Since the complex protocol probes a wider range of voltages and time scales, it has much greater power in constraining the model parameters. Unlike parameter sets from the first example, parameter sets from the second example produce  $I_{K_r}$  currents that appear almost identical under all three test protocols. In addition, the activation curves appear physiological. However, the  $I$ - $V$  curves are not physiological at voltages near  $-80$  mV. Information on the behavior of  $I_{K_r}$  at these voltages is needed to develop a more physiological model, but measuring  $I_{K_r}$  in native myocytes at these voltages is confounded by other contaminating currents. Panel c

shows the results from the third cost function. In this case, all parameter sets produce physiological currents. In addition, these currents are nearly identical, except for during the 60 mV activating pulse (Panel c, bottom). All five currents exhibit qualitatively similar inactivation during this pulse, due to the inclusion of the inactivation features from section “[Term 3: Inactivation](#)” in the cost function. However, since no quantitative training data recorded at 60 mV are included in the cost function (again, due to contaminating effects of other cardiac ion currents), small differences in the model currents are observed during the activating pulse.

To further test the results from the third cost function, we incorporated the resulting Markov type  $I_{K_r}$  models into a canine ventricular myocyte action



potential model<sup>14</sup> by replacing its original Hodgkin–Huxley type  $I_{K_r}$  model. We then simulated action potentials at various cycle lengths, and measured both the  $I_{K_r}$  currents and the action potentials (Fig. 6). The different parameter sets produce very similar results, as the maximal difference in peak current compared to the mean is 10%, and the maximal difference in action potential duration compared to the mean is 1.5%.

As illustrated by these examples, the parameter estimation method described in section “Methods” does not necessarily yield a unique parameter set. However, multiple parameter sets resulting from optimization reproduce the training data and also produce physiological, nearly identical currents under other conditions. With control  $I_{K_r}$  kinetics well constrained by this method, we next apply the method to identify drug binding parameters using  $I_{K_r}$  data recorded in the presence of verapamil.

#### Blocking of $I_{K_r}$ by Verapamil

It is known that the inhibition of an ion channel by a compound often depends on voltage, depolarization time, and/or frequency. The protocol described in

section “Electrophysiology” was designed to expose changes in drug block with respect to three variables: the first segment reveals dependency on the repolarization voltage, the second varies the depolarizing voltage, and the third exposes dependency of the effect of the drug on the duration of the depolarization pulse. Before developing models of the interaction of verapamil with the  $I_{K_r}$  current, we first test if the protocol reveals changes in the effect of the drug with respect to these three variables. For simplicity, we choose two out of the ten sweeps from each segment, and calculate the ratio of post-drug peak tail current to control peak tail current for both sweeps in each segment. We then apply a two-way ANOVA test for each segment.<sup>1</sup> We select the two sweeps by first identifying all sweeps that result in peak currents large enough to detect, and then choose the sweeps with the largest difference in the independent variable (voltage or time). Table 1 shows the ratio of post-drug peak tail currents to control peak tail currents from sweeps 1 (V11) and 8 (V18) for segment 1, sweeps 1 (V21) and 5 (V25) for segment 2, and sweeps 2 (T2) and 10 (T10) for segment 3, under 4 doses of verapamil (0.2, 2, 3, 5  $\mu\text{M}$ ). For each condition, three cell samples were collected. The results from

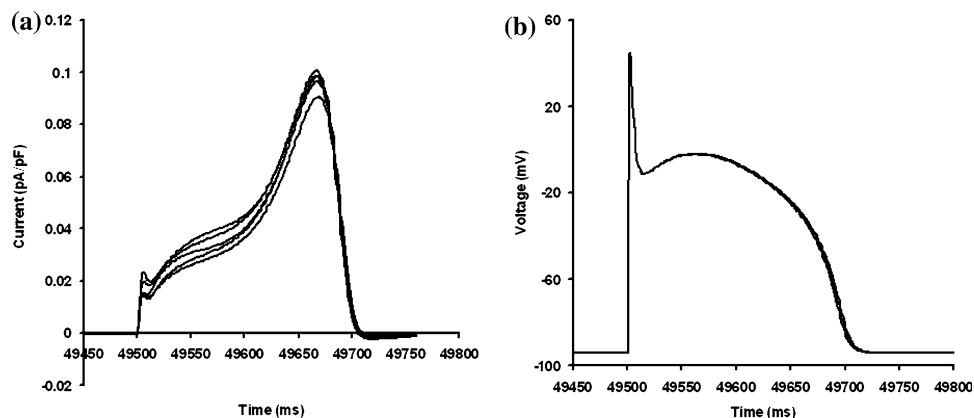


**FIGURE 6.** Action potential simulations. 5 accepted models from fitting to data under the complex protocol plus the two qualitative constraints in an action potential model<sup>14</sup> at a cycle length of 500 ms. In order to produce action potential durations similar to the original model, all 5 Markov type models were scaled by a factor of 5. (a)  $I_{K_r}$  currents. (b) Action potentials.

**TABLE 1.** Verapamil block of  $I_{K_r}$  is voltage dependent.

		0.2 $\mu\text{M}$		2 $\mu\text{M}$		3 $\mu\text{M}$		5 $\mu\text{M}$					
$p1$ 0.024	V11	0.83	0.85	1	0.5	0.44	0.27	0.48	0.48	0.43	0.35	0.42	0.14
	V18	0.4	0.89	1	0.45	0.28	0.11	0.23	0.38	0	0.18	0.18	0.08
$p2$ 0.0008	V21	0.60	0.88	1	0.41	0.31	0.23	0.32	0.38	0.33	0.22	0.25	0.26
	V25	1	1	1	0.58	0.53	1	0.38	0.48	0.68	0.35	0.58	0.42
$p3$ 0.126	T2	0.76	1	1	0.40	0.59	0.47	0.38	0.47	0.36	0.32	0.40	0.35
	T10	0.58	0.78	1	0.51	0.56	0.20	0.29	0.39	0.26	0.32	0.41	0.18

Ratio of post-drug peak tail to control peak tail currents are shown in the right four blocks. Data in the same column come from the same cell. V11 and V18 refer to sweeps 1 and 8 for segment 1, V21 and V25: sweeps 1 and 5 for segment 2; T2 and T10: sweeps 2 and 10 for segment 3.  $p$  values from the two-way ANOVA test are shown in the left most column. A  $p$  value  $<0.05$  is considered significant.

the ANOVA tests for each segment are listed in the leftmost column. A  $p$  value  $<0.05$  is considered significant. These data show that the inhibition of  $I_{Kr}$  by verapamil depends significantly on both the depolarization and repolarization voltage, with a  $p$  value of 0.0008 and 0.024, respectively, but does not seem to change with prolongation of the depolarization step ( $p$  value = 0.126).

### $I_{Kr}$ -Verapamil Models

We next study  $I_{Kr}$ -verapamil models from 12 different cell samples: three cells for each dose. Each  $I_{Kr}$ -verapamil model is generated by using training data from a particular cell. One or more parameter sets results from each optimization. Figure 7 illustrates a typical result. Figure 7a compares the model results to the training data for tail currents of the third sweep both under control and at a verapamil concentration of 2  $\mu$ M. Figures 7b and 7c shows sweeps 5 and 7; the model reproduces the control  $I_{Kr}$  kinetics and the effect of verapamil.

As cells differ from each other, so do models generated from data from different cells. Figure 8 shows the activation curves,  $I$ - $V$  curves, and binding and unbinding rates for all 12 best fits (some of the fittings yielded multiple acceptable parameter sets which have almost identical activation and  $I$ - $V$  curves, hence only the best fit is shown here), as well as representative tail current recordings for all cells. The variability in model parameters corresponds to observed cell-to-cell variability in the measured currents (see Data Supplement for parameter values for each model).

We next use the verapamil- $I_{Kr}$  models to explore the use- and frequency-dependent block of  $I_{Kr}$  by verapamil. Three different methods are used to predict the rate- and use-dependence of verapamil from the models. First, all 12 models (generated from data from all 12 cells) are simulated, producing a range of predictions. Second, 3 data sets at the same dose were averaged, and a single model is produced by estimating parameters using four averaged data sets simultaneously. Third, the 12 parameter sets are averaged to produce a single model. This method assumes that the model parameters vary independently from one cell to the next. As shown in Fig. 9, results from all three methods are qualitatively similar: verapamil block is both use- and rate-dependent, as inhibition of the current increases with both the number of pulses and at faster rates. These behaviors cannot be reproduced by using an  $IC_{50}$  value to modify the conductance of the current based on drug concentration. The model shown in Fig. 9c (from averaging the 12 parameter sets) exhibits a stronger drug effect than the model in Fig. 9b because it has a significantly larger binding

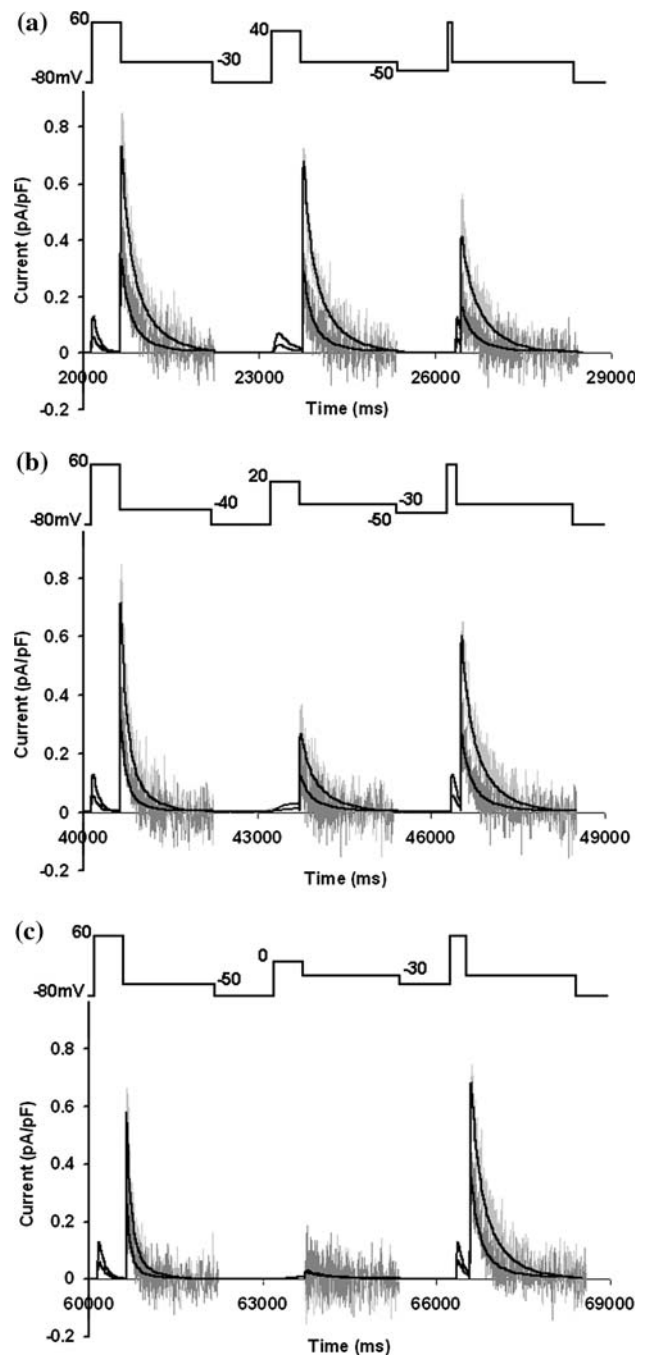


**FIGURE 7.** Comparison of model to data. Each subfigure shows one sweep. (a) Sweep 3; (b) sweep 5; (c) sweep 7. Training data under control are shown in light gray, data under steady state 2 $\mu$ M verapamil effect are shown in dark gray. Model generated traces are in black. Protocol of each sweep is shown on top.

rate; averaging the parameters biases the result toward larger values (see the Data Supplement for parameter values). A significant benefit of the first method is that it produces a range of predicted results that matches the variability of the cells used to generate the models.

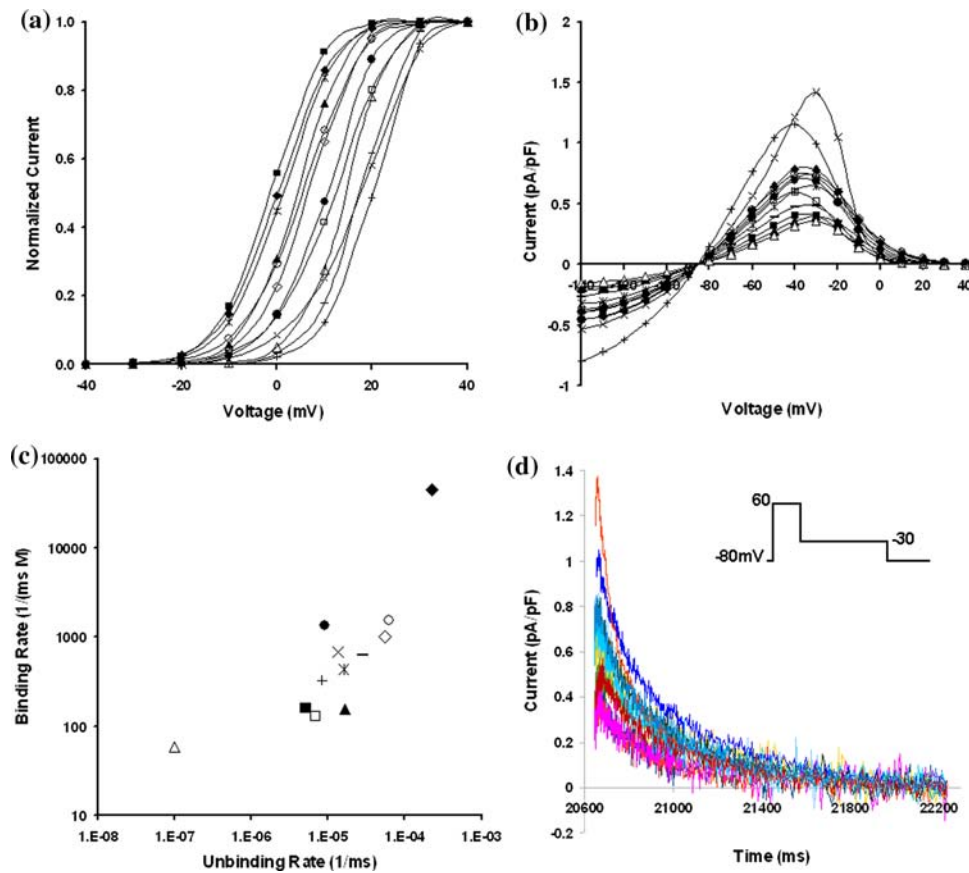


FIGURE 8. Properties of all models generated from cell samples. A specific symbol is used for each model. Same symbol in a, b, and c refer to same model. (a) Activation curve. (b)  $I$ - $V$  relations. (c) Binding rate vs. unbinding rate. (d) Tail currents of all cell samples at  $-30$  mV (protocol shown as inset).

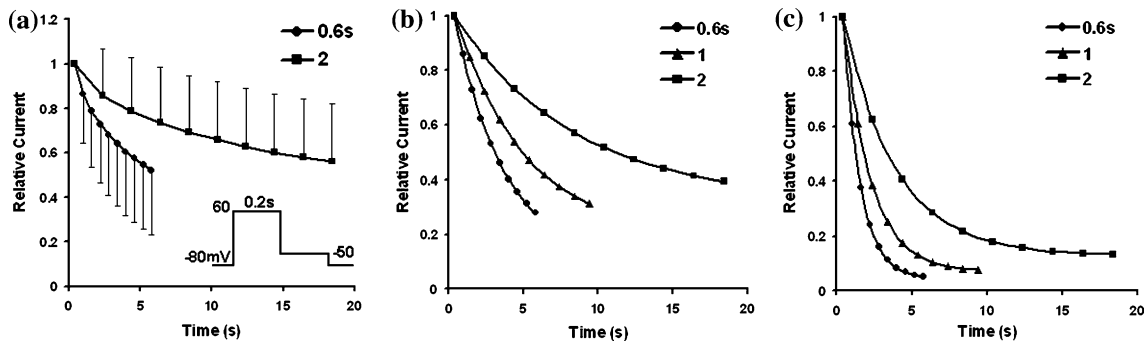


FIGURE 9. Use and frequency dependent block of  $I_{Kr}$  by  $2 \mu\text{M}$  verapamil. Trains of pulse protocol<sup>52</sup> as shown in the inset were applied at intervals of 0.6, 1, and 2 s. Normalized peak tail current is plotted vs. time. (a) Mean and SD (Standard Deviation) of all model predictions. SD is shown one-sided for clarity. Results for the 1-s interval not shown for clarity. (b) Prediction of the model from fitting to the averaged data. (c) Prediction of the model from the averaged parameters.

Finally, we take advantage of the form of the Markov model to relate the observed time scale of the onset of drug block from the use-dependence simulations to time scales that can be calculated directly from the model. For a fixed value of voltage, the equations

of the model are linear. Thus, we can find the steady-state solution as well as the eigenvalues (and therefore time constants) of the system as a function of voltage. The system has five degrees of freedom, and therefore five time constants. Figure 10 shows the two largest

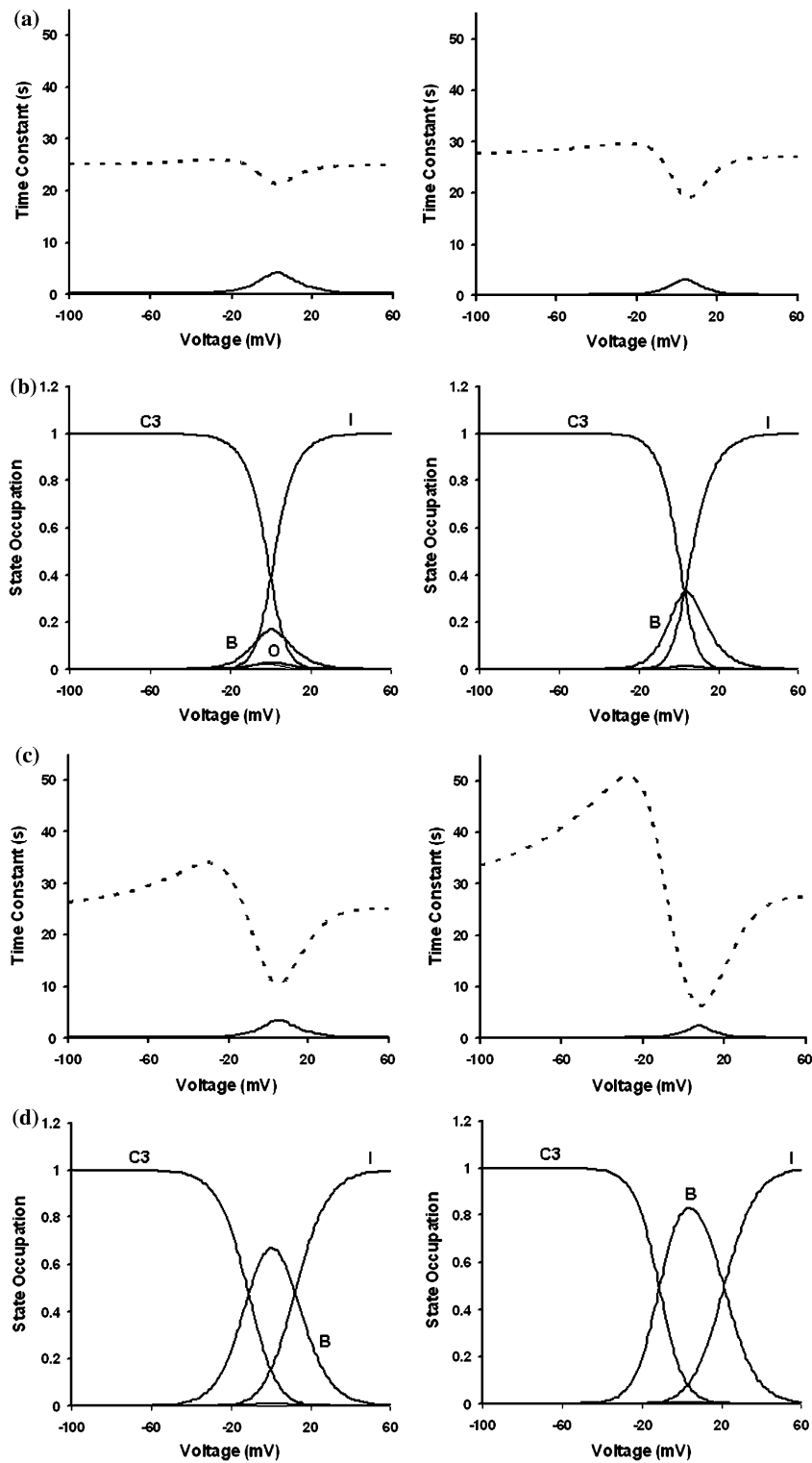


FIGURE 10. Time scale and state occupation vs. voltage. (a) Time constants at 0.2 uM; (b) State occupation at 0.2 uM; (c) Time constants at 2 uM; (d) State occupation at 2 uM. Left panel: model from the averaged data. Right panel: model from averaging the parameters.

time constants as a function of voltage for two doses (a and b: 0.2 uM, c and d: 2 uM) and two models (left: model from averaged data, right: model from averaged

parameters). The other three time constants are very fast compared to the two largest and therefore not shown. The dashed line represents the time scale



associated with the action of the drug. This time scale is faster at those voltages where the drug bound state of the channel is maximal. Comparing Figs. 10a to 10c, the time scale over this voltage range decreases with increasing drug concentration. Furthermore, the model in Fig. 10, left, has smaller drug bound state than that shown in Fig. 10, right, which corresponds to the weaker effect of drug block in Fig. 9b as compared to Fig. 9c.

## DISCUSSION

This paper presents a method for developing mathematical models of the effect of a drug on native  $I_{Kr}$ . This method incorporates two types of information about  $I_{Kr}$ : time series recordings of the current and qualitative features of the current from published studies. One term in the cost function used to estimate model parameters includes recordings of  $I_{Kr}$  using a complex voltage protocol designed to probe voltage- and time-dependence. Data from the first and third iterations of the protocol are used for parameter estimation: during control, and when the effect of the drug had reached its full extent. Including data from these two iterations produces models that can reproduce native channel kinetics, and that capture the steady-state dose-dependent changes in the current due to the compound. An important aspect of the method is the inclusion of qualitative features of the current to further constrain parameter estimation and to produce physiological results for conditions in which it is difficult to measure  $I_{Kr}$  in myocytes. Thus, the method generates models that reproduce “typical” features of  $I_{Kr}$  but also reproduce behavior specific to  $I_{Kr}$  from the cell (or group of cells) that were used to estimate model parameters. The two qualitative features used in this study are  $I$ - $V$  relations and inactivation. When the method is applied to other channels, one may need to choose different qualitative features to constrain a certain model appropriately. While global optimization may result in more than one parameter set, the method developed here produces parameter sets that behave quite similarly. This method is computationally intensive, yet it is practical using relatively modest clusters (one optimization took about 12 h using 29 processors).

Although the dependence of the model output (namely the current) is a nonlinear function of the system parameters, the model used in this investigation is a piecewise linear system, if piecewise constant voltage protocols and drug concentrations are chosen. While solving linear systems is conceptually (though not necessarily numerically) straightforward and results in a sum of exponential functions, estimating

time constants and coefficients in a sum of exponentials is notoriously difficult.<sup>20</sup> Thus, the particular model studied here is a worthy example system. Extending the method to a model that is a nonlinear dynamical system may be more difficult, since the cost function landscape may well be more complex. Still, the method itself does not require an underlying linear system. Thus, the method presented here is general and can be applied to study other ion currents.

One choice for investigators using this method involves how to use models that result from a number of cells. The results presented here explored three possibilities: averaging all of the data to generate a single “average model” from the data, generating a model for each cell and then averaging the parameters in those models to generate an “average” model, or generating a model for each cell, and then studying the whole population of models in subsequent simulations (see Fig. 9). A benefit in using all model samples is that it allows one to generate predictions about the variability of a result, which is similar to the approach taken in many experimental studies. If an investigator desires a single model for studying qualitative features of a compound’s effect on  $I_{Kr}$ , an averaged model can be used; as shown in Fig. 9, all three methods produced qualitatively similar results. Developing models specific to a particular cell or group of cells presents an interesting potential strategy for exploring functional differences in  $I_{Kr}$  in different cardiac cell types, in different species, or due to genetic variants. These differences are known to have important consequences in the presence of certain compounds.<sup>36</sup>

Application of this method requires an initial estimate of the model structure and parameters. If no accurate model of the current under study exists, then the method presented here can complement computational techniques for addressing the issue of model identifiability that have been discussed by others.<sup>4,7</sup> For example, the method can be helpful in discriminating between different model topologies. It can also help identify the state-specific action of a drug on a channel, such as which state or states it might bind, or if the drug binding rate might be voltage dependent. If two possible topologies yield significantly different cost values after optimization, the one with lower cost could be considered the more likely structure. In the example we studied, the block of  $I_{Kr}$  by verapamil is rate-dependent, suggesting open or inactivated state block.<sup>52</sup> The results presented here assumed that the drug binds to the open state; we also investigated models in which the drug bound to the inactive state. Optimization using models with binding to the inactive state yielded similar minimum cost values as well as similar simulation results to model structures with drug binding to the open state. Thus, for the purposes

of this study verapamil may bind to either the open or inactive state, with similar functional effects. These results are consistent with experimental observations that suggest that verapamil could bind to either the open or inactive state.<sup>52</sup>

Finally, verapamil is an interesting test compound because although it is a potent  $I_{Kr}$  inhibitor, it does not appear to pose a risk for inducing acquired Long QT Syndrome or Torsades de Pointes.<sup>36</sup> Verapamil is a multi-channel inhibitor; its effects on other currents, such as the L-type calcium current and the late sodium current, may be protective.<sup>51,52</sup> An interesting future direction of this work would be to develop similar strategies for generating data-driven models of the effect of compounds on the other major cardiac ion currents, and then to use these models to link the multi-channel activity of compounds such as verapamil to the effect of the compound on the ventricular action potential.

## APPENDIX

Calculating the expectation of fluctuations in the cost function caused by noise in the experimental recordings:  $\Delta c$ .

$N$  Number of data points in the training data  
 $T_i$  Training data at the  $i$ th data point  
 $S_i$  Simulation value at the  $i$ th data point  
 $R_i$  Real value of data (without noise) at the  $i$ th data point  
 $n_i$  Noise at the  $i$ th data point  
 $c$  Cost function  
 $\sigma^2$  Standard deviation of Gaussian noise. This derivation assumes we know  $\sigma^2$ . To estimate it, we take 600 data points ( $d_i$ ) at the beginning of each sweep when the voltage is at resting potential, shift them so the average of these 600 points is 0, and calculate the normalized average of each point squared across all sweeps, i.e.,

$$\sigma^2 = \frac{1}{6000} \sum_{i=1}^{6000} d_i^2.$$

$\langle \rangle$  calculating expectation

$$\begin{aligned} c &= \frac{1}{N} \sum_{i=1}^N (T_i - S_i)^2 = \frac{1}{N} \sum_{i=1}^N (R_i + n_i - S_i)^2 \\ &= \frac{1}{N} \sum_{i=1}^N \left[ (R_i - S_i)^2 + n_i^2 + 2n_i(R_i - S_i) \right] \end{aligned}$$

$$\begin{aligned} \langle c \rangle &= \frac{1}{N} \left\langle \sum_{i=1}^N \left[ (R_i - S_i)^2 + n_i^2 + 2n_i(R_i - S_i) \right] \right\rangle \\ &= \frac{1}{N} \sum_{i=1}^N (R_i - S_i)^2 + \frac{1}{N} \left\langle \sum_{i=1}^N n_i^2 \right\rangle \\ &\quad + \frac{2}{N} \left\langle \sum_{i=1}^N n_i(R_i - S_i) \right\rangle = \frac{1}{N} \sum_{i=1}^N (R_i - S_i)^2 + \sigma^2 \end{aligned}$$

$$\langle c \rangle^2 = \frac{1}{N^2} \left[ \sum_{i=1}^N (R_i - S_i)^2 \right]^2 + \sigma^4 + \frac{2}{N} \sigma^2 \sum_{i=1}^N (R_i - S_i)^2$$

$$\begin{aligned} \langle c^2 \rangle &= \left\langle \frac{1}{N^2} \left( \sum_{i=1}^N \left[ (R_i - S_i)^2 + n_i^2 + 2n_i(R_i - S_i) \right] \right)^2 \right\rangle \\ &= \frac{1}{N^2} \left\langle \left[ \sum_{i=1}^N (R_i - S_i)^2 \right]^2 + \left[ \sum_{i=1}^N n_i^2 \right]^2 \right. \\ &\quad \left. + \left[ \sum_{i=1}^N 2n_i(R_i - S_i) \right]^2 + 2 \left[ \sum_{i=1}^N (R_i - S_i)^2 \right] \left[ \sum_{i=1}^N n_i^2 \right] \right\rangle \\ &\quad + \frac{1}{N^2} \left\langle 2 \left[ \sum_{i=1}^N (R_i - S_i)^2 \right] \left[ \sum_{i=1}^N 2n_i(R_i - S_i) \right] \right. \\ &\quad \left. + 2 \left[ \sum_{i=1}^N 2n_i(R_i - S_i) \right] \left[ \sum_{i=1}^N n_i^2 \right] \right\rangle \\ &= \frac{1}{N^2} \left[ \sum_{i=1}^N (R_i - S_i)^2 \right]^2 + \left\langle \frac{1}{N^2} \left[ \sum_{i=1}^N n_i^2 \right]^2 \right\rangle \\ &\quad + \frac{4}{N} \sigma^2 \sum_{i=1}^N (R_i - S_i)^2 + \frac{2}{N} \sigma^2 \sum_{i=1}^N (R_i - S_i)^2 \end{aligned}$$

$$\begin{aligned} \Delta c^2 &= \langle c^2 \rangle - \langle c \rangle^2 \\ &= \left\langle \frac{1}{N^2} \left[ \sum_{i=1}^N n_i^2 \right]^2 \right\rangle + \frac{4}{N} \sigma^2 \sum_{i=1}^N (R_i - S_i)^2 - \sigma^4 \end{aligned}$$

For a lower bound on  $\Delta c^2$ , take  $R_i = S_i$ ,

$$\begin{aligned} \Delta c^2 &= \left\langle \frac{1}{N^2} \left[ \sum_{i=1}^N n_i^2 \right]^2 \right\rangle - \sigma^4 \\ &= \left\langle \frac{1}{N^2} \sum_{i=1}^N n_i^4 + \frac{2}{N^2} \sum_{i=1}^N \sum_{i' \neq i}^N n_i^2 n_{i'}^2 \right\rangle - \sigma^4 \\ &= \frac{1}{N} \langle n_i^4 \rangle + \left( 1 - \frac{1}{N} \right) \langle n_i^2 n_{i'}^2 \rangle - \sigma^4 = \frac{\langle n_i^4 \rangle}{N} - \frac{\sigma^4}{N} \end{aligned}$$

$$\langle n_i^4 \rangle = \int_{-\infty}^{+\infty} n^4 \frac{e^{-n^2/2\sigma^2}}{\sqrt{2\pi\sigma^2}} dn = 2 \int_0^{+\infty} n^4 \frac{e^{-n^2/2\sigma^2}}{\sqrt{2\pi\sigma^2}} dn$$

Let  $x = n^2/2\sigma^2$

$$\langle n_i^4 \rangle = \frac{4\sigma^4}{\sqrt{\pi}} \int_0^{+\infty} x^{3/2} e^{-x} dx = \frac{4\sigma^4}{\sqrt{\pi}} \Gamma\left(\frac{5}{2}\right) = 3\sigma^4$$

Hence:

$$\Delta c = \sqrt{\frac{2\sigma^4}{N}} = \sigma^2 \sqrt{\frac{2}{N}}$$

## ELECTRONIC SUPPLEMENTARY MATERIAL

The online version of this article (doi: [10.1007/s10439-009-9690-5](https://doi.org/10.1007/s10439-009-9690-5)) contains supplementary material, which is available to authorized users.

## ACKNOWLEDGMENTS

The authors acknowledge support from NIH Grant R44 HL07793, NIH Grant R01 HL075515, and NSF Grant DGE-0333366. We thank Dr. Robert F. Gilmour, Jr. at Cornell University for insightful comments and suggestions, as well as our colleagues at Gene Network Sciences for their invaluable contributions, in particular to Steve Penrod for help with Visual Cell software. We also thank Dr. Randall Rasmusson at University at Buffalo for his comments. Finally, we thank the reviewers for helpful suggestions that improved the manuscript.

## REFERENCES

- <sup>1</sup><http://rweb.stat.umn.edu/cgi-bin/Rweb/buildModules.cgi>.
- <sup>2</sup>Anson, B. D., M. J. Ackerman, D. J. Tester, M. L. Will, B. P. Delisle, C. L. Anderson, and C. T. January. Molecular and functional characterization of common polymorphisms in HERG (KCNH2) potassium channels. *Am. J. Physiol. Heart Circ. Physiol.* 286:H2434–H2441, 2004. doi:[10.1152/ajpheart.00891.2003](https://doi.org/10.1152/ajpheart.00891.2003).
- <sup>3</sup>Antzelevitch, C., L. Belardinelli, A. C. Zygmunt, A. Burashnikov, J. M. Di Diego, J. M. Fish, J. M. Cordeiro, and G. Thomas. Electrophysiological effects of ranolazine, a novel antiarrhythmic agent with antiarrhythmic properties. *Circulation* 110:904–910, 2004. doi:[10.1161/01.CIR.0000139333.83620.5D](https://doi.org/10.1161/01.CIR.0000139333.83620.5D).
- <sup>4</sup>Bauer, R. J., B. F. Bowman, and J. L. Kenyon. Theory of the kinetic analysis of patch-clamp data. *Biophys. J.* 52:961–978, 1987. doi:[10.1016/S0006-3495\(87\)83289-7](https://doi.org/10.1016/S0006-3495(87)83289-7).
- <sup>5</sup>Bottino, D., R. C. Penland, A. Stamps, M. Traebert, B. Dumotier, A. Georgieva, G. Helmlinger, and G. S. Lett. Preclinical cardiac safety assessment of pharmaceutical compounds using an integrated systems-based computer model of the heart. *Prog. Biophys. Mol. Biol.* 90:414–443, 2006. doi:[10.1016/j.pbiomolbio.2005.06.006](https://doi.org/10.1016/j.pbiomolbio.2005.06.006).
- <sup>6</sup>Clancy, C. E., Z. I. Zhu, and Y. Rudy. Pharmacogenetics and anti-arrhythmic drug therapy: a theoretical investigation. *Am. J. Physiol. Heart Circ. Physiol.* 292:H66–H75, 2007. doi:[10.1152/ajpheart.00312.2006](https://doi.org/10.1152/ajpheart.00312.2006).
- <sup>7</sup>Colquhoun, D. Agonist-activated ion channels. *Brit. J. Pharmacol.* 147:s17–s26, 2006. doi:[10.1038/sj.bjp.0706502](https://doi.org/10.1038/sj.bjp.0706502).
- <sup>8</sup>Cordeiro, J. M., L. Greene, C. Heilmann, D. Antzelevitch, and C. Antzelevitch. Transmural heterogeneity of calcium activity and mechanical function in the canine left ventricle. *Am. J. Physiol. Heart Circ. Physiol.* 286:H1471–H1479, 2004. doi:[10.1152/ajpheart.00748.2003](https://doi.org/10.1152/ajpheart.00748.2003).
- <sup>9</sup>Cordeiro, J. M., J. E. Malone, J. M. Di Diego, F. S. Scornik, G. L. Aistrup, C. Antzelevitch, and J. A. Wasserstrom. Cellular and subcellular alternans in the canine left ventricle. *Am. J. Physiol. Heart Circ. Physiol.* 293:H3506–H3516, 2007. doi:[10.1152/ajpheart.00757.2007](https://doi.org/10.1152/ajpheart.00757.2007).
- <sup>10</sup>Crumb, W., and I. Caverio. QT interval prolongation by non-cardiovascular drugs: issues and solutions for novel drug development. *Pharmaceut. Sci. Technol.* 2:270–280, 1999. doi:[10.1016/S1461-5347\(99\)00172-8](https://doi.org/10.1016/S1461-5347(99)00172-8).
- <sup>11</sup>Davie, C., J. Pierre-Valentin, C. Pollard, N. Standen, J. Mitcheson, P. Alexander, and B. Thong. Comparative pharmacology of guinea pig cardiac myocyte and cloned hERG (I(Kr)) channel. *J. Cardiovasc. Electrophysiol.* 15:1302–1309, 2004. doi:[10.1046/j.1540-8167.2004.04099.x](https://doi.org/10.1046/j.1540-8167.2004.04099.x).
- <sup>12</sup>Fermini, B., and A. A. Fossa. The impact of drug-induced QT interval prolongation on drug discovery and development. *Nat. Rev. Drug Discov.* 2:439–447, 2003. doi:[10.1038/nrd1108](https://doi.org/10.1038/nrd1108).
- <sup>13</sup>Floudas, C., and P. Pardalos. Recent advances in global optimization. Princeton, NJ: Princeton University Press, 1992.
- <sup>14</sup>Fox, J. J., J. L. McHarg, and R. F. Gilmour, Jr. Ionic mechanism of electrical alternans. *Am. J. Physiol.* 282:H516–H530, 2002.
- <sup>15</sup>Friedrichs, G. S., L. Patmore, and A. Bass. Non-clinical evaluation of ventricular repolarization (ICH S7B): results of an interim survey of international pharmaceutical companies. *J. Pharmacol. Toxicol. Methods* 52:6–11, 2005. doi:[10.1016/j.vascn.2005.05.001](https://doi.org/10.1016/j.vascn.2005.05.001).
- <sup>16</sup>Haverkamp, W., G. Breithardt, A. J. Camm, M. J. Janse, M. R. Rosen, C. Antzelevitch, D. Escande, M. Franz, M. Malik, A. Moss, and R. Shah. The potential for QT prolongation and pro-arrhythmia by non-anti-arrhythmic drugs: clinical and regulatory implications. Report on a Policy Conference of the European Society of Cardiology. *Cardiovasc. Res.* 47:219–233, 2000. doi:[10.1016/S0008-6363\(00\)00119-X](https://doi.org/10.1016/S0008-6363(00)00119-X).
- <sup>17</sup>Hille, B. *Ionic Channels of Excitable Membranes*. Sunderland, Mass.: Sinauer Associates, Inc., 1992.
- <sup>18</sup>Hodgkin, A. L., and A. F. Huxley. A quantitative description of membrane current and its application to conduction and excitation in nerve. *J. Physiol.* 117:500–544, 1952.
- <sup>19</sup>Hund, T. J., and Y. Rudy. Rate dependence and regulation of action potential and calcium transient in a canine cardiac ventricular cell model. *Circulation* 110:3168–3174, 2004. doi:[10.1161/01.CIR.0000147231.69595.D3](https://doi.org/10.1161/01.CIR.0000147231.69595.D3).
- <sup>20</sup>Istratov, A. A., and O. F. Vyvenko. Exponential analysis in physical phenomena. *Rev. Sci. Instrum.* 70:1233–1257, 1999. doi:[10.1063/1.1149581](https://doi.org/10.1063/1.1149581).

- <sup>21</sup>Iyer, V., R. Mazhari, and R. L. Winslow. A computational model of the human left-ventricular epicardial myocyte. *Biophys. J.* 87:1507–1525, 2004. doi:[10.1529/biophysj.104.043299](https://doi.org/10.1529/biophysj.104.043299).
- <sup>22</sup>Keener, J. P., and J. Sneyd. *Mathematical Physiology*. New York: Springer, 1998.
- <sup>23</sup>Kiehn, J., A. E. Lacerda, and A. M. Brown. Pathways of HERG inactivation. *Am. J. Physiol. Heart Circ. Physiol.* 277:H199–H210, 1999.
- <sup>24</sup>Kirsch, G. E., E. S. Trepakova, J. C. Brimacombe, S. S. Sidach, H. D. Erickson, M. C. Kochan, L. M. Shyjka, A. E. Lacerda, and A. M. Brown. Variability in the measurement of hERG potassium channel inhibition: effects of temperature and stimulus pattern. *J. Pharmacol. Toxicol. Methods* 50:93–101, 2004. doi:[10.1016/j.vascn.2004.06.003](https://doi.org/10.1016/j.vascn.2004.06.003).
- <sup>25</sup>Kiss, L., P. B. Bennett, V. N. Uebele, K. S. Koblan, S. A. Kane, B. Neagle, and K. Schroeder. High throughput ion-channel pharmacology: planar-array-based voltage clamp. *Assay Drug Dev. Technol.* 1:127–135, 2003. doi:[10.1089/154065803762851298](https://doi.org/10.1089/154065803762851298).
- <sup>26</sup>Liu, S., R. L. Rasmusson, D. L. Campbell, S. Wang, and H. C. Strauss. Activation and inactivation kinetics of an E-4031 sensitive current (IKr) from single ferret atrial myocytes. *Biophys. J.* 70:2704–2715, 1996. doi:[10.1016/S0006-3495\(96\)79840-5](https://doi.org/10.1016/S0006-3495(96)79840-5).
- <sup>27</sup>Lu, Y., M. P. Mahaut-Smith, A. Varghese, C. L.-H. Huang, P. R. Kemp, and J. I. Vandenberg. Effects of premature stimulation on HERG K<sup>+</sup> channels. *J. Physiol.* 537:843–851, 2001. doi:[10.1113/jphysiol.2001.012690](https://doi.org/10.1113/jphysiol.2001.012690).
- <sup>28</sup>Marquardt, D. An algorithm for least-squares estimation of nonlinear parameters. *Siam J. Appl. Math.* 11:431–441, 1963. doi:[10.1137/0111030](https://doi.org/10.1137/0111030).
- <sup>29</sup>Mazhari, R., J. L. Greenstein, R. L. Winslow, E. Marban, and H. B. Nuss. Molecular interactions between two long-QT syndrome gene products, HERG and KCNE2, rationalized by in vitro and in silico analysis. *Circ. Res.* 89:33–38, 2001. doi:[10.1161/hh1301.093633](https://doi.org/10.1161/hh1301.093633).
- <sup>30</sup>Milescu, L. S., G. Akk, and F. Sachs. Maximum likelihood estimation of ion channel kinetics from macroscopic currents. *Biophys. J.* 88:2494–2515, 2005. doi:[10.1529/biophysj.104.053256](https://doi.org/10.1529/biophysj.104.053256).
- <sup>31</sup>Noble, D., and Y. Rudy. Models of cardiac ventricular action potentials iterative interaction between experiment and simulation. *Phil. Trans. Roy. Soc. (Lond)* 359:1127–1142, 2001. doi:[10.1098/rsta.2001.0820](https://doi.org/10.1098/rsta.2001.0820).
- <sup>32</sup>Nocedal, J. and S. J. Wright. *Numerical Optimization*. Springer, 2006.
- <sup>33</sup>Press, W. H., S. A. Teukolsky, W. T. Vetterling, and B. P. Flannery. *Numerical Recipes in C*. Cambridge, UK: Cambridge University Press, 1992.
- <sup>34</sup>Rampe, D., B. Wible, D. Fedida, R. C. Dage, and A. M. Brown. Verapamil blocks a rapidly activating delayed rectifier K<sup>+</sup> channel cloned from human heart. *Mol. Pharmacol.* 44:642–648, 1993.
- <sup>35</sup>Rand, D. G., Q. Zhou, G. T. Buzzard, and J. J. Fox. Computationally efficient strategy for modeling the effect of ion current modifiers. *IEEE Trans. Biomed. Eng.* 55:3–13, 2008. doi:[10.1109/TBME.2007.896594](https://doi.org/10.1109/TBME.2007.896594).
- <sup>36</sup>Redfern, W. S., L. Carlsson, A. S. Davis, W. G. Lynch, I. MacKenzie, S. Palethorpe, P. K. Siegl, I. Strang, A. T. Sullivan, R. Wallis, A. J. Camm, and T. G. Hammond. Relationships between preclinical cardiac electrophysiology, clinical QT interval prolongation and torsade de pointes for a broad range of drugs: evidence for a provisional safety margin in drug development. *Cardiovasc. Res.* 58:32–45, 2003. doi:[10.1016/S0008-6363\(02\)00846-5](https://doi.org/10.1016/S0008-6363(02)00846-5).
- <sup>37</sup>Ridley, J. M., J. T. Milnes, Y. H. Zhang, H. J. Witchel, and J. C. Hancox. Inhibition of HERG K<sup>+</sup> current and prolongation of the guinea-pig ventricular action potential by 4-aminopyridine. *J. Physiol.* 549:667–672, 2003. doi:[10.1113/jphysiol.2003.043976](https://doi.org/10.1113/jphysiol.2003.043976).
- <sup>38</sup>Roden, D. M. Mechanisms and management of proarrhythmia. *Am. J. Cardiol.* 82:491–571, 1998. doi:[10.1016/S0002-9149\(98\)00472-X](https://doi.org/10.1016/S0002-9149(98)00472-X).
- <sup>39</sup>Sanguinetti, M. C., and P. B. Bennett. Antiarrhythmic drug target choices and screening. *Circ. Res.* 93:491–499, 2003. doi:[10.1161/01.RES.0000091829.63501.A8](https://doi.org/10.1161/01.RES.0000091829.63501.A8).
- <sup>40</sup>Sanguinetti, M. C., C. Jiang, M. E. Curran, and M. T. Keating. A mechanistic link between an inherited and an acquired cardiac arrhythmia: HERG encodes the IKr potassium channel. *Cell* 81:299–307, 1995. doi:[10.1016/0092-8674\(95\)90340-2](https://doi.org/10.1016/0092-8674(95)90340-2).
- <sup>41</sup>Shiferaw, Y., M. A. Watanabe, A. Garfinkel, J. N. Weiss, and A. Karma. Model of intracellular calcium cycling in ventricular myocytes. *Biophys. J.* 85:3666–3686, 2003. doi:[10.1016/S0006-3495\(03\)74784-5](https://doi.org/10.1016/S0006-3495(03)74784-5).
- <sup>42</sup>Shunn, C. D. Evaluating goodness-of-fit in comparison of models to data. [www.lrdc.pitt.edu/schunn/gof/GOF.doc](http://www.lrdc.pitt.edu/schunn/gof/GOF.doc).
- <sup>43</sup>Snyders, D. J., and A. Chaudhary. High affinity open channel block by dofetilide of HERG expressed in a human cell line. *Mol. Pharmacol.* 49:949–955, 1996.
- <sup>44</sup>Starmer, C. F., A. Grant, and H. C. Strauss. Mechanisms of use-dependent block of sodium channels in excitable membranes by local anesthetics. *Biophys. J.* 46:15–17, 1984. doi:[10.1016/S0006-3495\(84\)83994-6](https://doi.org/10.1016/S0006-3495(84)83994-6).
- <sup>45</sup>Storn, R. *On the Usage of Differential Evolution for Function Optimization*. Berkeley: NAFIPS, 1996.
- <sup>46</sup>Tanskanen, A. J., J. L. Greenstein, B. O'Rourke, and R. L. Winslow. The role of stochastic and modal gating of cardiac L-type Ca<sup>2+</sup> channels on early after-depolarizations. *Biophys. J.* 88:85–95, 2005. doi:[10.1529/biophysj.104.051508](https://doi.org/10.1529/biophysj.104.051508).
- <sup>47</sup>ten Tusscher, K. H., D. Noble, P. J. Noble, and A. V. Panfilov. A model for human ventricular tissue. *Am. J. Physiol. Heart Circ. Physiol.* 286:H1573–H1589, 2004. doi:[10.1152/ajpheart.00794.2003](https://doi.org/10.1152/ajpheart.00794.2003).
- <sup>48</sup>Trudeau, M. C., J. W. Warmke, B. Ganetzky, and G. A. Robertson. HERG, a human inward rectifier in the voltage-gated potassium channel family. *Science* 269:92–95, 1995. doi:[10.1126/science.7604285](https://doi.org/10.1126/science.7604285).
- <sup>49</sup>Waltman, P. *A Second Course in Elementary Differential Equations*. Orlando: Academic Press, 1996.
- <sup>50</sup>Wang, S., S. Liu, M. J. Morales, H. C. Strauss, and R. L. Rasmusson. A quantitative analysis of the activation and inactivation kinetics of HERG expressed in *Xenopus* oocytes. *J. Physiol.* 502:45–60, 1997. doi:[10.1111/j.1469-7793.1997.045bl.x](https://doi.org/10.1111/j.1469-7793.1997.045bl.x).
- <sup>51</sup>Zhang, S., T. Sawanobori, Y. Hirano, and M. Hiraoka. Multiple modulations of action potential duration by different calcium channel blocking agents in guinea pig ventricular myocytes. *J. Cardiovasc. Pharmacol.* 30:489–496, 1997. doi:[10.1097/00005344-199710000-00013](https://doi.org/10.1097/00005344-199710000-00013).
- <sup>52</sup>Zhang, S., Z. Zhou, Q. Gong, J. C. Makielski, and C. T. January. Mechanism of block and identification of the verapamil binding domain to HERG potassium channels. *Circ. Res.* 84:989–998, 1999.